Atmos. Chem. Phys., 14, 1663–1677, 2014
www.atmos-chem-phys.net/14/1663/2014/
doi:10.5194/acp-14-1663-2014

Atmospheric Chemistry and Physics Open Access

Temporal changes in the emissions of CH_4 and CO from China estimated from CH_4 / CO_2 and CO / CO_2 correlations observed at Hateruma Island

Y. Tohjima[1], M. Kubo[2], C. Minejima[3], H. Mukai[1], H. Tanimoto[1], A. Ganshin[4], S. Maksyutov[1], K. Katsumata[1], T. Machida[1], and K. Kita[2]

[1]Center for Global Environmental Research, National Institute for Environmental Studies, Tsukuba, Japan
[2]Faculty of Science, Ibaraki University, Mito, Japan
[3]Department of Chemical Engineering, Tokyo University of Agriculture and Technology, Tokyo, Japan
[4]Central Aerological Observatory, Dolgoprudny, Russia

Correspondence to: Y. Tohjima (tohjima@nies.go.jp)

Received: 22 August 2013 – Published in Atmos. Chem. Phys. Discuss.: 30 August 2013
Revised: 18 December 2013 – Accepted: 8 January 2014 – Published: 13 February 2014

Abstract. In situ observation of the atmospheric CO_2, CH_4, and CO mixing ratios at Hateruma Island (HAT, 24.05° N, 123.80° E) often show synoptic-scale variations with correlative elevations during winter, associated with air transport from the East Asian countries. We examine winter (November–March) trends in $\Delta CH_4 / \Delta CO_2$, $\Delta CO / \Delta CO_2$, and $\Delta CO / \Delta CH_4$ observed at Hateruma over the period 1999 to 2010. To investigate the relationship between the East Asian emissions and the short-term variations in the atmospheric mixing ratios, we use the FLEXPART Lagrangian particle dispersion model (LPDM). The observed ratios $\Delta CH_4 / \Delta CO_2$ and $\Delta CO / \Delta CO_2$ both show an overall gradual decrease over the study period due to a recent rapid increase in fossil fuel consumption in China. We note, however, that the decreasing rates of $\Delta CH_4 / \Delta CO_2$ and $\Delta CO / \Delta CO_2$ show gradual decrease and increase, respectively, during the entire observation periods used in this study. The $\Delta CO / \Delta CH_4$ slope, on the other hand, shows an increasing trend during 1999–2004 but a decrease during 2005–2010. Calculation of the concentration footprint for the atmospheric observation at HAT by using the FLEXPART LPDM indicates that most of the short-term variations are caused by emission variations from northern and eastern China. Combined with a set of reported emission maps, we have estimated the temporal changes in the annual CH_4 and CO emissions from China under the assumption that the estimate of the fossil-fuel-derived CO_2 emissions based on the energy statistics are accurate. The estimated annual CH_4 emissions, corresponding to nonseasonal sources or anthropogenic sources without rice fields, show a nearly constant value of 39 ± 7 TgCH$_4$ yr^{-1} during 1998–2002, and then gradually increase to 46 ± 8 TgCH$_4$ yr^{-1} in 2009/2010. The estimated annual CO emissions increase from 134 ± 32 TgCO yr^{-1} in 1998/1999 to 182 ± 42 TgCO yr^{-1} in 2004/2005, level off after 2005, and then slightly decrease to less than 160 TgCO yr^{-1} in 2008–2010.

1 Introduction

Methane (CH_4) is the second-most-important anthropogenic greenhouse gas in the atmosphere after carbon dioxide (CO_2). Analyses of ancient air occluded in polar ice core samples have suggested that atmospheric CH_4 has more than doubled since the preindustrial period (e.g., Etheridge et al., 1998; Nakazawa et al., 1993). This long-term increase can be attributed to increases in anthropogenic sources (e.g., fossil fuels, domestic ruminants, and rice fields). Recent systematic measurements of atmospheric CH_4 have shown a slowing down in the rate of increase after the 1980s with a significant interannual variability (Steele et al., 1992; Dlugokencky et al., 1998), leveling off in the early 2000s (Dlugokencky et al., 2003), and an abrupt renewed increase after 2007 (Rigby et al., 2008; Dlugokencky et al., 2009; Terao et al., 2011).

These temporal changes in atmospheric CH_4 are a result of an overall balance between the emission and loss processes that include soil absorption and chemical reactions with atmospheric hydroxyl radical (OH) and stratospheric $O(^1D)$ and Cl atoms.

Carbon monoxide (CO), produced during incomplete combustion of fossil fuels and biomass and the oxidation of atmospheric CH_4 and nonmethane volatile organic compounds (NMVOC), is an atmospheric pollutant. CO also plays an important role in atmospheric chemistry. The CO reaction with OH, a dominant sink for atmospheric CO, removes about 75 % of OH in the atmosphere (Thompson, 1992), influencing the atmospheric oxidation capacity. Therefore, changes in the CO emission could indirectly affect the atmospheric levels of CH_4 and other species that are removed by OH (e.g., Logan et al., 1981). Depending on the levels of the mixing ratios of nitrogen oxides (NO_x), CO acts as a source for tropospheric ozone, which is also a greenhouse gas. Since both CH_4 and CO have the potential to affect directly and indirectly the global climate, it is crucial to understand their changing emissions with time by obtaining better spatiotemporal information about their surface fluxes.

In terms of regional emissions of greenhouse gases and air pollutants, East Asia is one of the most important regions in the world because of the positive association between anthropogenic emissions and the recent rapid economic growth in the region (e.g., Emission Database for Global Atmospheric Research (EDGAR) v4.2 (EC-JRC/PBL, 2011); Carbon Dioxide Information Analysis Center (CDIAC) (Boden et al., 2011); Regional Emission inventory in ASia (REAS) v2.1; Kurokawa et al., 2013). For example, fossil-fuel-derived CO_2 emissions in China, based on the CDIAC database, have more than doubled over the recent decade (Fig. 1), and surpassed the United States as the world's largest fossil CO_2 emitter in 2006 (Gregg et al., 2008). The increases in the fossil CO_2 emissions from China will also likely lead to enhanced emissions of other chemical species related to fossil fuel combustion. The recently revised EDGAR v4.2 shows an increase in the estimated anthropogenic CH_4 and CO emissions from China after 2003 (Fig. 1b and c). These increases are mostly related to CH_4 from coal mining and CO from the sectors of industrial manufacturing and metal production. However, the CH_4 and CO emission inventories are considered to be more uncertain than the fossil CO_2 emission inventory because those emissions related to complete combustion are generally well estimated while the emissions related to incomplete combustion and agricultural activities are poorly constrained (Kurokawa et al., 2013). These emission increases will result in a corresponding elevation in the mixing ratios of CH_4, CO, and CO_2 in the downwind region of the sources.

Downward from the source regions, a synoptic-scale variation (SSV) in the mixing ratio of one chemical species is usually associated with SSVs of other species that have similar regional emission distributions and atmospheric lifetime characteristics. Therefore, various combinations of specific chemical species with relatively well quantified sources or relationships can be used to constrain emission estimates of other species with poorly quantified source strengths. For example, atmospheric Radon-222 measurements have been used to constrain regional fluxes of such greenhouse gases as CO_2 and CH_4 (e.g., Levin et al., 2003; Schmidt et al., 2003; Wada et al., 2013). Worthy et al. (2009) estimated the interannual variation in anthropogenic CH_4 emissions from Europe and Siberia based on the CH_4 / CO_2 correlations observed at Alert, Canada. Yokouchi et al. (2006) estimated the emission strength of hydrofluorocarbons and halocarbons from East Asian countries based on their correlations with atmospheric CO observed at Hateruma Island.

The National Institute for Environmental Studies (NIES) has been carrying out in situ measurements of atmospheric greenhouse gases and pollutants including CO_2, CH_4, and CO at Hateruma Island (HAT; 24.05° N, 123.80° E), which is located off the coast of continental East Asia. During the period from late fall to early spring, HAT is mainly influenced by the air masses transported from East Asian countries, resulting in highly associated SSV events of enhanced mixing ratios of atmospheric CO_2, CH_4 and CO. Using the observed CO_2 and CH_4 SSVs at HAT during winter (November–April), Tohjima et al. (2010) found that the ratio of the standard deviations of deseasonalized CO_2 and CH_4 ($\sigma_{CO_2} / \sigma_{CH_4}$) gradually increased during 1996–2007, reflecting changes in the fossil CO_2 emissions from China.

In this study, in addition to revisiting the analysis of CO_2 and CH_4 at HAT, we have extended our study to include an analysis of the correlation between CO and CO_2 by using hourly data instead of daily averages, as was done in a previous study by Tohjima et al. (2010). Here we examine 24 h variations based on the hourly data because shorter-term variations are likely to reflect more directly the regional emissions from the East Asian countries. By calculating the temporal variations in the ratios of $\Delta CH_4 / \Delta CO_2$, $\Delta CO / \Delta CO_2$, and $\Delta CO / \Delta CH_4$ from the observed measurements at HAT over the period from 1997/1998 to 2010, and combining them with the footprint results for different gases from a Lagrangian particle dispersion model (FLEXPART) and the existing flux maps of CH_4, CO and CO_2, we are able to improve the estimate of the spatiotemporal distributions of these trace gases and their source strengths in continental Asia.

2 In situ observation at Hateruma Island

We have been monitoring atmospheric CO_2, CH_4 and CO at HAT by using automated analytical systems, which have been described elsewhere by Mukai et al. (2001) for CO_2, by Tohjima et al. (2002) for CH_4, and Tanimoto et al. (2009) for CO. Therefore, we give only a brief description of these analytical systems.

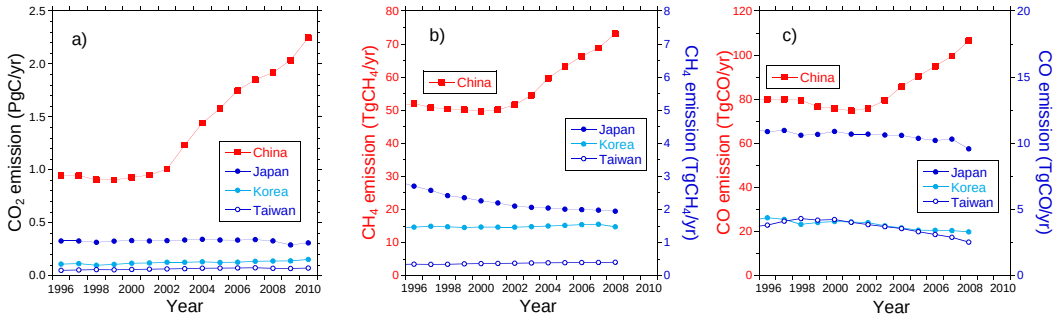

Fig. 1. Temporal changes in the estimated emissions of **(a)** fossil-fuel-derived CO_2, **(b)** CH_4, and **(c)** CO from China, Japan, Korea, and Taiwan. The CO_2 emissions are taken from the CDIAC database. CH_4 and CO emissions are taken from EDGAR v4.2. CH_4 and CO emissions from Japan, Korea and Taiwan are plotted against the right *y* axis.

Two air intakes (inverted cylindrical beakers), one for CO_2 and the other for CH_4 and CO measurements, are placed at the top of a tower at a height of 36.5 m (46.5 m a.s.l.), and sample air is drawn in through a 3 / 8-inch stainless-steel tubing by diaphragm pumps placed inside the station building.

The sample air for CO_2 measurement is dried by passing it through 3 cold traps (2 °C, −40 °C and −70 °C). CO_2 is continuously measured by a nondispersive infrared analyzer (NDIR) (URA207, Shimadzu CO. Ltd., Japan) with an analytical precision of about 0.02 µmol mol^{-1} (ppm). CO_2 mixing ratios are determined against 4 working standard gases, each a mixture of cleanup air and pure CO_2 filled in a 49 L aluminum cylinder. The cleanup air is made from natural air by passing it through a cold trap to reduce water vapor, a heated Pt catalyst to oxidize CO and hydrocarbons into CO_2 and water vapor, and a molecular sieve 5A column to remove CO_2 and residual water vapor. The CO_2 mixing ratios of the 4 working standard gases span about 50 ppm, and fully cover the range of atmospheric variations observed at HAT. These 4 working standard gases are replaced every 2–2.5 yr, and their mixing ratios are calibrated against the NIES 09 CO_2 standard scale (Machida et al., 2011) in our laboratory before and after every use at HAT. Before and after differences are less than 0.05 ppm.

To reduce water vapor in the sample air for CH_4 and CO measurements, we use a Nafion® tube dryer and a cold trap (−40 °C). The dried air is then introduced into the CH_4 and CO analytical systems, separately. CH_4 and CO are semicontinuously measured by a gas chromatograph equipped with a flame ionization detector (GC/FID) and a gas chromatograph/mercury oxide (GC / HgO) analyzer (RGA3, Trace Analytical Co. Ltd., USA), respectively. The analytical precisions are about 2 nmol mol^{-1} (ppb) for both CH_4 and CO measurements. The GC analysis interval for CH_4 and CO is 10 min, except during January 1996–November 1997, when the interval was 15 min for CH_4. Thus the CH_4 data before November 1997 are not used in this study because of the lower analysis frequency. Both the CH_4 and CO mixing ratios are determined against the working standard gases, each made up of a mixture of cleanup air and pure CH_4 or CO gases filled in a 49 L aluminum cylinder. These CH_4 and CO working standards are traceable to the NIES 94 CH_4 standard scale (Terao et al., 2011) and the NIES 09 CO standard scale (Katsumata et al., 2011), respectively.

For CH_4 measurements, we use 3 working standard gases with mixing ratios of about 1700, 1850, and 2000 ppb. Each set of 3 working standard gases are replaced every 5 yr at HAT. After December 2009, we have changed the volume of the working gas cylinder to 9.4 L, and have replaced the working standard gases every year. We have yet to observe any significant drift in these CH_4 working standard gases during use at HAT.

For CO measurements, we use 3 working standard gases with mixing ratios of about 80 ppb, 200 ppb and 400 ppb for the period 1999 to 2004. After September 2004, we have added a 4th CO standard gas with a mixing ratio of about 800 ppb. The procedural protocol for the CO working gas is similar to that of the CH_4 working gas, and after December 2009 we have been using 9.4 L aluminum cylinders, instead of the 49 L cylinders, and are replacing them every year. Unfortunately, the working standards in all the 49 L aluminum cylinders except one showed significant drifts, ranging from 1 to 16 ppb yr^{-1}. The drifts in the CO working reference gases during use at HAT have been determined in our laboratory by linear or quadratic interpolation based on the temporal changes in the CO mixing ratios before and after use at HAT. In order to validate the interpolated CO mixing ratios of the working standard gases, we compare the in situ observation with flask sample measurements, which are collected primarily for O_2 / N_2 measurements at HAT (Tohjima et al., 2008). The CO mixing ratios from flask samples are measured by using a GC / HgO analyzer at our laboratory. The average and the standard deviation of the differences between the flask data and the corresponding in situ hourly data are 0.3 ppb and 7.0 ppb, respectively, with 89 % of the differences lying within a range of ±10 ppb (Fig. S1 in the Supplement); the slope of the correlation plot is 1.008 ± 0.003

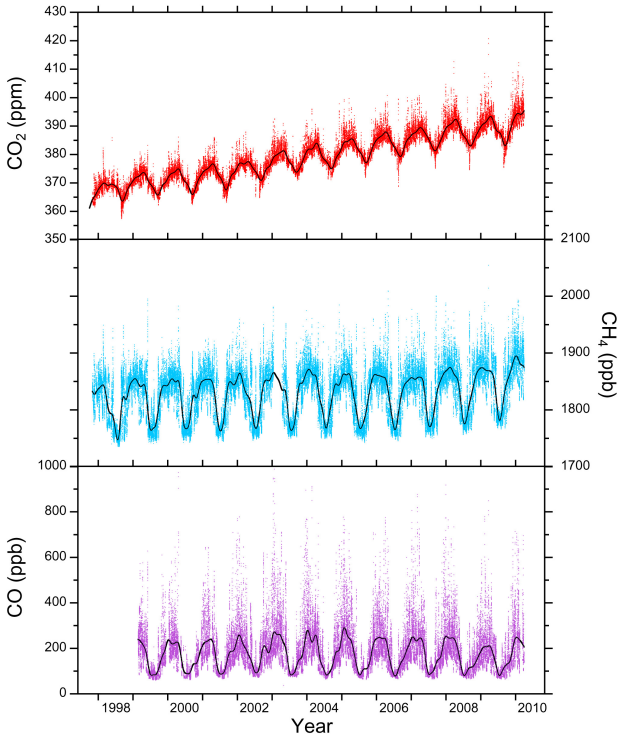

Fig. 2. Time series of atmospheric (top) CO_2, (middle) CH_4, and (bottom) CO mixing ratios observed at HAT. Each dot represents hourly average. Black lines represent the smooth curve fits to the data.

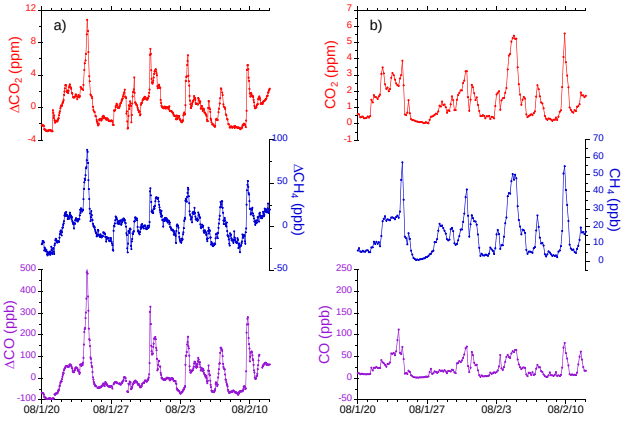

Fig. 3. Synoptic scale variations in hourly (top) CO_2, (middle) CH_4, and (bottom) CO based on **(a)** the observation and **(b)** the model simulation for the period from 20 January to 12 February 2008. The range of the y axis for the simulation plot for each chemical species is half of that for the corresponding observation plot.

(Fig. S2), giving confidence to the ability of our interpolation to accurately reflect the drift.

For this study, we use hourly averages of the atmospheric CO_2, CH_4, and CO mixing ratios observed at HAT for the correlation analysis. The study periods are from November 1997 to March 2010 for CO_2 and CH_4, and from November 1998 to March 2010 for CO (Fig. 2).

3 Methods of correlation analysis

Our focus is on the temporal change in the correlational relationship between CO_2, CH_4, and CO associated with synoptic-scale variations (SSVs) observed at HAT. Our calculation procedure begins with obtaining a best-fit smooth curve to each of the time series by using the methods of Thoning et al. (1989) with a cut-off frequency of 4.6 cycles yr^{-1}, and then subtracting it from the original time series. The residual time series are denoted as ΔCO_2, ΔCH_4 and ΔCO. The hourly ΔCO_2, ΔCH_4, and ΔCO time series from 20 January to 11 February in 2008 are shown in Fig. 3a as a typical example. We have also calculated the best-fit smooth curves by using cut-off frequencies of 2.3 and 9.2 cycles yr^{-1} and have found that the average $\Delta CH_4 / \Delta CO_2$, $\Delta CO / \Delta CO_2$, and $\Delta CO / \Delta CH_4$ slopes (see Sect. 5.1) for the 3 different cut-off frequencies agree to within 1 %.

We then construct scatter plots of ΔCH_4 vs. ΔCO_2, ΔCO vs. ΔCO_2, and ΔCO vs. ΔCH_4 using the first 24 h of data. Reduced major axis (RMA) regression analysis is carried out on each scatter plot to obtain regression slopes ($\Delta CH_4 / \Delta CO_2$, $\Delta CO / \Delta CO_2$, and $\Delta CO / \Delta CH_4$ slopes) (Hirsh and Gilroy, 1984). We repeat the RMA analysis as we successively shift the 24 h time window by 1 h over the entire data record. If (i) the absolute value of the correlation coefficient is less than 0.8 ($|R| < 0.8$), or (ii) the number of data is less than 5, or (iii) the standard deviation of CO_2 is less than 0.1 ppm ($1\sigma_{CO_2} < 0.1$), then we deem the regression slope to be statistically insignificant and do not include it in the calculation of monthly averages of the correlation slopes. The RMA analysis is a relatively robust method of calculating the slope of two variables which show some causative relationship. Although we arbitrarily choose the correlation coefficient of 0.8 as a rough criterion for selecting significant correlation slopes, it should be noted that the average correlation slopes of $\Delta CH_4 / \Delta CO_2$, $\Delta CO / \Delta CO_2$, and $\Delta CO / \Delta CH_4$, as discussed in Sect. 5.1, do depend slightly on the value of the criterion. These average slopes for $|R| < 0.7$, $|R| < 0.8$ and $|R| < 0.9$ are plotted in Fig. S3. The root mean squares of the overall differences in the average regression slopes for $|R| < 0.7$ and $|R| < 0.9$ from those for $|R| < 0.8$ are 2.5 %, 2.3 %, and 3.4 % for $\Delta CH_4 / \Delta CO_2$, $\Delta CO / \Delta CO_2$, and $\Delta CO / \Delta CH_4$, respectively.

Figure 4 shows the average seasonal variation of the regression slopes. In the figure, each closed circle denotes the monthly average for the whole observation period, each error bar represents the standard deviation, and each black bar shows the number of regression slopes used to calculate the monthly average. The negative values of the average

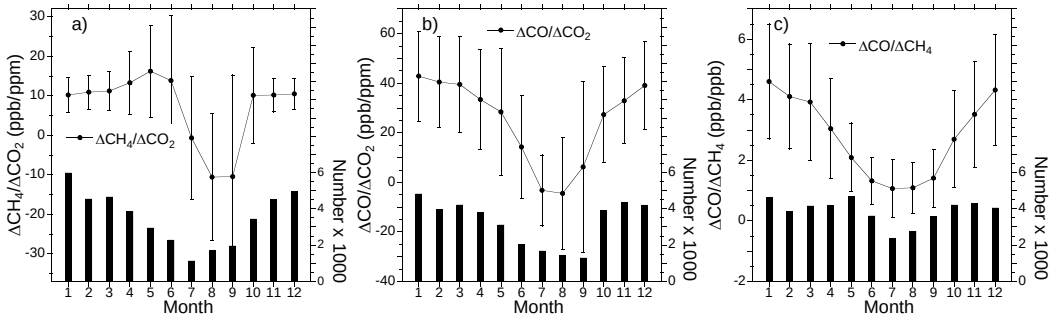

Fig. 4. Average seasonal variation of **(a)** $\Delta CH_4 / \Delta CO_2$, **(b)** $\Delta CO / \Delta CO_2$, and **(c)** $\Delta CO / \Delta CH_4$ slopes observed at HAT. The error bars represent the standard deviations from the monthly averages. The vertical bars represent the data number.

$\Delta CH_4 / \Delta CO_2$ and $\Delta CO / \Delta CO_2$ slopes in the summer are due to contribution from the enhanced terrestrial CO_2 uptake. We also note that the seasonal variation in the average $\Delta CO / \Delta CH_4$ slope may be attributable mainly to the seasonality in the air mass transport. During the summer, air masses arriving at HAT are predominantly transported from the Pacific region and the contributions of the Southeast Asian emissions show a relative increase. (Fig. S4 shows the average footprint, which is discussed in Sect. 4.1, during the summer period (May to September)). Thus the average $\Delta CO / \Delta CH_4$ slope is low in summer because the CO / CH_4 emission ratios for the Southeast Asian countries are lower than those for China, Japan and Korea (e.g., Kurokawa et al., 2013). However, it is possible that the seasonality in the emissions from East Asia, the maximum CH_4 emissions in summer (Yan et al., 2003) and the maximum CO emissions in winter (Streets et al., 2003; Zhang et al., 2009), and the significantly faster CO reaction with OH in summer could partially contribute to the seasonality in the average $\Delta CO / \Delta CH_4$ slope.

The number of regression slopes with high correlation coefficients ($|R| > 0.8$) decreases during the summer due to the predominant influence of maritime air masses from the Pacific at HAT (see Fig. S4). During the winter, fluxes from East Asia contribute to the short-term variations observed at HAT. But the monthly average slopes, especially $\Delta CH_4 / \Delta CO_2$, are relatively constant from late autumn to early spring (from November to March), when the biotic activity is relatively dormant. These results seem to suggest that the emissions from East Asia during the 5-month winter period are relatively constant in time.

We now proceed to examine in detail the interannual variations in the correlation slopes observed at HAT during the 5-month winter period from November to March. Note that the 2006/2007 winter, for example, indicates the period from November 2006 to March 2007. The 5-month winter period used for this study is shorter than the 6-month winter period (November to April) used in a previous study by Tohjima et al. (2010).

4 Model simulation of correlation slopes

4.1 Concentration footprint for the measurements at HAT

In order to investigate the relationship between regional emissions and the correlation slopes observed at HAT, we employ FLEXPART v8.0 (Stohl et al., 1998), a Lagrangian particle dispersion model. The model has been used to simulate the SSVs at HAT for CO_2 (Koyama et al., 2011), and for CO_2 and O_2 (Minejima et al., 2012). We compute concentration footprints that indicate the degree of sensitivity of each measurement to the surface fluxes upwind of the measurement site (HAT). To drive FLEXPART, we use 6-hourly meteorology data with a spatial resolution of $1.25° \times 1.25°$ from the JMA Climate Data Assimilation System (JCDAS) provided by the Japan Meteorological Agency (JMA). In each model run, 10 000 particles are released from 36.5 m a.g.l. at HAT and transported back 8 days, giving enough time for particles to spread over East Asia. Footprints are prepared on a $0.5° \times 0.5°$ grid for 1, 2, 3, ..., 8 days back in time with a time resolution of 3 h from January 2006 to December 2010. Details of the model and simulation condition are described in Ganshin et al. (2012, 2013).

The average footprint for HAT during the 5-month winter period is shown in Fig. 5. The distribution of the footprint clearly shows that the emissions from East Asia have significant influence on the observation at HAT. The average correlation slopes from the model are determined mostly by the emissions from the area with footprint larger than 1×10^{-4} ppm $(\mathrm{gC\,m^{-2}\,day^{-1}})^{-1}$. Therefore, the area confined by the 1×10^{-4} ppm $(\mathrm{gC\,m^{-2}\,day^{-1}})^{-1}$ contour line is referred to hereafter as an effective footprint area (EFA) for the measurements at HAT. EFA includes northern China, eastern China, Korea, western Japan, and Taiwan.

4.2 Flux maps used in the model simulations

As part of the simulation procedure, we use fossil CO_2 emissions (fossil fuel burning and cement production) from

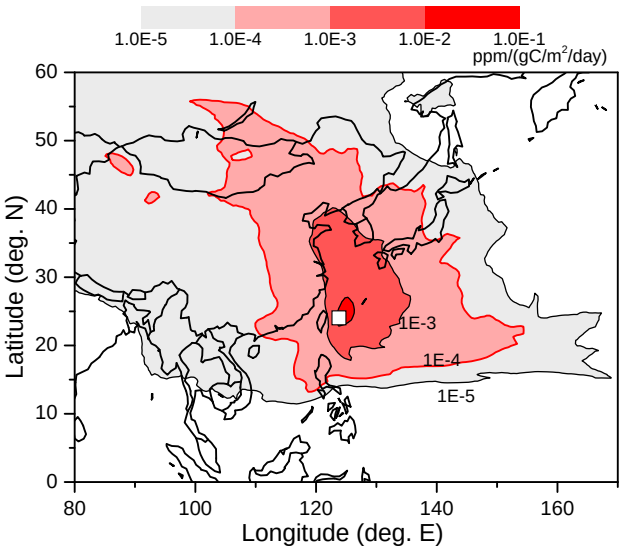

Fig. 5. Average footprint (ppm $(\mathrm{gC\,m^{-2}\,day^{-1}})^{-1}$) for the measurements at HAT during the winter period (November to March). Meteorological data for 2006–2010 are used for the calculation. The location of HAT is indicated by the square. The area surrounded by the red thick contour lines of 1×10^{-4} ppm $(\mathrm{gC\,m^{-2}\,day^{-1}})^{-1}$ is defined as an effective footprint area (EFA).

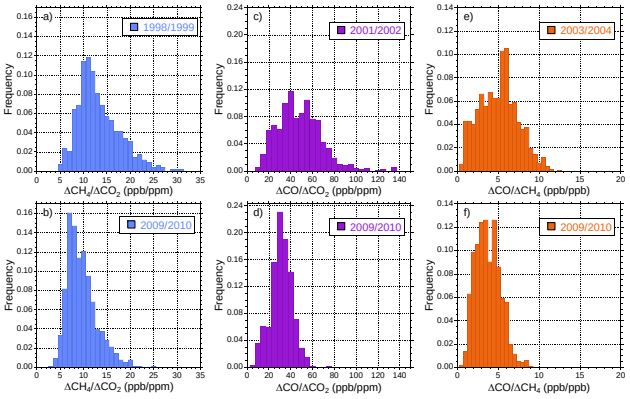

Fig. 6. Histograms of the correlation slopes of (**a**, **b**) $\Delta CH_4 / \Delta CO_2$, (**c**, **d**) $\Delta CO / \Delta CO_2$, and (**e**, **f**) $\Delta CO / \Delta CH_4$ for the selected two periods. The correlation slopes all meet the selection criteria (see text).

the EDGAR v4.2 CO_2 annual flux data (excluding short-cycle organic carbon from biomass burning) with a grid of $0.1° \times 0.1°$ for the period 1997 to 2008. For our study, the spatial resolution of these annual fluxes is decreased to $0.5° \times 0.5°$. The emissions from China, Japan, Korea, Taiwan and the residual regions are then scaled to the national emission inventories from CDIAC (Boden et al., 2011) for the corresponding years. The fossil CO_2 flux maps for 2009 and 2010 are extrapolated from the 2008 EDGAR v4.2 emission map.

In addition to the fossil CO_2 fluxes, climatological monthly fluxes of the terrestrial biosphere from the optimized CASA (Carnegie–Ames–Stanford Approach) ecosystem model (Nakatsuka and Maksyutov, 2009) and of the oceanic air–sea exchange from Takahashi et al. (2009) are used. These data have a spatial resolution of $1° \times 1°$, and are applied year after year (no interannual variation) for simulating the atmospheric CO_2 SSVs at HAT.

For CH_4, we use the monthly CH_4 emission maps gridded at $1° \times 1°$ for 2007 taken from the emission scenario (E2 scenario) developed in Patra et al. (2009). Simulated atmospheric CH_4 mixing ratios in a transport model using these CH_4 emission maps generally agree with the observed global distribution and seasonality (Patra et al., 2009). We use the above CH_4 emission maps due to their technical ease of use and suitability, and not the CH_4 emission maps from the EDGAR v4.2 database because it only provides the annual flux maps. For CO, we use the EDGAR v4.2 CO annual flux maps gridded at $0.1° \times 0.1°$ for 2007. The spatial resolution of the CO flux map is decreased to a resolution of $0.5° \times 0.5°$.

In order to examine the influence of different emission databases on the concentration fields in a transport model, we also use anthropogenic CO_2 emission distributions from the Open-source Data Inventory of Anthropogenic CO_2 Emission (ODIAC) v3.0, which was originally developed by Oda and Maksyutov (2011) and modified by Maksyutov et al. (2013), and the recently revised REAS v2.1 (Kurokawa et al., 2013; http://www.nies.go.jp/REAS/), and CH_4 and CO emission distributions from REAS v2.1. Although both ODIAC v3.0 and REAS v2.1 provide monthly emission maps, annually averaged emission maps for CO_2 and CO are used for the simulation comparisons. The CO_2 emissions from China, Japan, Korea, and Taiwan contained in the ODIAC and REAS v2.1 databases are scaled to the CDIAC national emission inventories, as was done for the EDGAR CO_2 emission maps. Similarly, the annually averaged CO emission maps for 2007 from REAS v2.1 are scaled to match the EDGAR national emissions for China, Japan, Korea, and Taiwan for 2007. The REAS v2.1 monthly CH_4 emission maps for 2007 are also scaled to match the monthly national emissions of Patra et al. (2009) for China, Japan, Korea, and Taiwan. The influence of these different emission maps on the correlation slopes are discussed in Sect. 5.2.

4.3 Simulation of SSVs of CO_2, CH_4, and CO and their correlation analysis

In this study, we have been able to compute concentration footprints from January 2006 to December 2010 using FLEXPART. We then multiply these concentration footprints with the abovementioned fluxes to produce simulated time series of SSVs corresponding to individual fluxes. Chemical destruction of CH_4 and CO by hydroxyl radical (OH) during transport from the source regions to the receptor (HAT) are

estimated by using OH concentration values at various latitudinal locations of the back trajectory in the boundary layer. The OH concentration data are obtained from the monthly climatological distributions of zonal mean OH (Spivakovsky et al., 2000). The reaction rate constants for CH_4 and CO with OH are obtained from the Jet Propulsion Laboratory database (Sander et al., 2006). Although the chemical reaction with OH does not significantly influence the simulated CH_4 concentration during its short transport time, it does reduce CO SSVs by about 5 % in the winter.

The simulated CO_2, CH_4, and CO variations for the same period as shown Fig. 3a are depicted in Fig. 3b. As can be seen in Fig. 3a and b, the model results are generally able to capture the observed pollution events with elevated mixing ratios. However, many of the details in the observed variations of the mixing ratios are not well reproduced, and the simulated amplitudes are generally underestimated, consistent with the results of previous studies (Koyama et al., 2011; Minejima et al., 2012). These discrepancies between the simulation and observation can be attributed to errors in the transport and/or fluxes used in the model simulation. A lack of variations of several days due to the timescale of large-scale air mass mixing might partially contribute to the apparent smaller-than-observed simulated variations because the filtering procedure mentioned in Section 3 cannot effectively remove such midrange variations. In this study, we have attempted to reduce the impact of transport errors by using correlation slopes to estimate regional emissions. It has been found that these correlation slopes are not strongly influenced by atmospheric transport under the assumption that the CO_2, CH_4 and CO fluxes have similar spatial distributions in East Asia (cf. Tohjima et al., 2010). To examine the robustness of this assumption, we compare the flux maps prepared in Sect. 4.2 (see Fig. S5). Since the strong emissions, primarily confined to the land areas, are generally distributed in the southern part of North China, east China, the Korean Peninsula, and Japan, we are confident that the spatial distributions of the CO_2, CH_4, and CO fluxes within EFA are roughly similar to each other.

In order to evaluate the relationship between the East Asian emissions and the correlation slopes during the winter period, we calculate average correlation slopes from the simulated 5 yr SSVs for various sets of the abovementioned emissions. The average correlation slopes are calculated as follows: time series of SSVs of CO_2 are obtained as a summed contribution from the fossil, oceanic, and land biotic CO_2 fluxes. From the simulated CH_4, CO, and combined CO_2 time series, we obtain correlation slopes of $\Delta CH_4 / \Delta CO_2$ and $\Delta CO / \Delta CO_2$, in the same way as the observed correlation slopes are calculated (see Sect. 3). We evaluate the winter average of the correlations slopes for the fossil emissions during 1998 to 2010 by using the corresponding time series of SSVs of the fossil CO_2. In this calculation, any influence of the year-to-year variation in the meteorological transport on the average correlation slopes appears as variability in the correlation slopes from the 5 yr simulated SSVs.

5 Results and discussion

5.1 Observed correlation slopes

Figure 6 shows the histograms of the correlation slopes derived from the observations made during the winter periods of 1998/1999 and 2009/2010 for $\Delta CH_4 / \Delta CO_2$, of 2001/2002 and 2009/2010 for $\Delta CO / \Delta CO_2$, and of 2003/2004 and 2009/2010 for $\Delta CO / \Delta CH_4$. These years are selected to highlight the extent of change in the distribution of the individual correlation slopes that has taken place over a decadal timescale. The correlation slopes of $\Delta CH_4 / \Delta CO_2$, $\Delta CO / \Delta CO_2$ and $\Delta CO / \Delta CH_4$ for the 2009/2010 winter have narrower distributions and lower average values than those of the earlier years. These changes are attributable to changes in the relative strengths of the emissions from EFA. The histograms of the correlation slopes of the simulated $\Delta CH_4 / \Delta CO_2$ and $\Delta CO / \Delta CO_2$ (see Sect. 5.2) show similar temporal changes to those in the observation: the distributions become narrow in association with the increase in the fossil-fuel-derived CO_2 emissions in China (see Fig. S6, in which the histogram of the simulated $\Delta CH_4 / \Delta CO_2$ for 1998/1999 and 2009/2010 and $\Delta CO / \Delta CO_2$ for 2001/2002 and 2009/2010 are depicted). Note that the histograms of the simulated $\Delta CH_4 / \Delta CO_2$ and $\Delta CO / \Delta CO_2$ driven by the 1998 fossil CO_2 emission map show a similar temporal change in the distribution, suggesting that the contribution of the change in the emission distribution is relatively small.

Temporal changes in the winter averages of the correlation slopes are depicted in Fig. 7. Tohjima et al. (2010) examined the interannual changes in the synoptic-scale variations of CO_2 and CH_4 at HAT during a 6-month period (November to April) of each year from 1996 to 2007, and found that the CO_2 variability gradually increased relative to that of CH_4. They attributed the gradual increase to the recent rapid increase in the fossil-fuel-derived CO_2 emissions from China (Gregg et al., 2008). Thus, the increase in the CO_2 variability has caused the average $\Delta CH_4 / \Delta CO_2$ and $\Delta CO / \Delta CO_2$ correlation slopes shown in Fig. 7 to decrease gradually with time. The observed $\Delta CH_4 / \Delta CO_2$ and $\Delta CO / \Delta CO_2$ slopes decrease from about 12 to less than 10 ppb ppm^{-1} and from about 45 to 30 ppb ppm^{-1} during 1998–2010, respectively. But the rate of decrease is gradually getting smaller for the $\Delta CH_4 / \Delta CO_2$ slope, while it is gradually getting larger for the $\Delta CO / \Delta CO_2$ slope during the whole observation periods. Unlike these trends, the average $\Delta CO / \Delta CH_4$ slope shows gradual increase during 1999–2004 and decrease during 2005–2010.

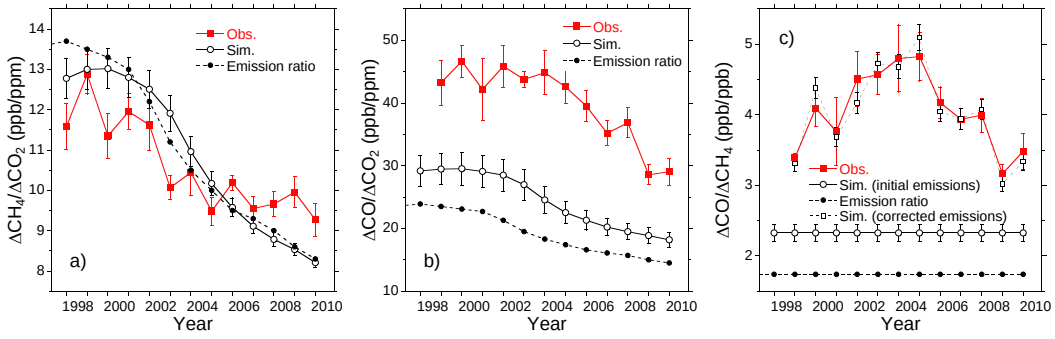

Fig. 7. Temporal changes in the winter average correlation slopes of **(a)** $\Delta CH_4 / \Delta CO_2$, **(b)** $\Delta CO / \Delta CO_2$, and **(c)** $\Delta CO / \Delta CH_4$. The red closed squares represent the observation and the open circles represent the simulation. The error bars represent the standard errors. The ratios of the emissions within EFA are also depicted as closed circles. The black open squares in Fig. 7c represent the $\Delta CO / \Delta CH_4$ slopes based on the optimized CH_4 and CO emissions from China within EFA (see text).

5.2 Simulated correlation slopes

As described in Sect. 4, we obtain correlation slopes from the simulated CO_2, CH_4, and CO SSVs, using time-varying fossil CO_2 emissions. In Fig. 7a and b, we also depict the winter averages of the simulated $\Delta CH_4 / \Delta CO_2$ and $\Delta CO / \Delta CO_2$ slopes. Both of the simulated slopes show similar decreasing trends. The temporal change in the simulated $\Delta CH_4 / \Delta CO_2$ slopes agrees well with the observed change, especially for the early period. However, the temporal decrease in the decreasing rate is not well simulated for the latter period. This discrepancy may be explained by the previously noted increase in the CH_4 emissions from EFA, since the model CH_4 field is driven by the fixed 2007 CH_4 monthly emission maps, while the CO_2 field is driven by the temporally varying CDIAC emission inventories.

The simulated $\Delta CO / \Delta CO_2$ slopes underestimate the observed slopes by about 30 % (Fig. 7b), suggesting that the CO / CO_2 emission ratio within EFA in the model is lower than the actual ratio. However, the overall decreasing trend pattern of the simulated $\Delta CO / \Delta CO_2$ slopes agrees generally with the observation. The simulated $\Delta CO / \Delta CH_4$ slope based on the fixed emissions is also about half of the observed slopes (Fig. 7c).

The winter averages of the CH_4 / CO_2, CO / CO_2, and CO / CH_4 ratios of the EFA emissions used in the simulations are also plotted in Fig. 7. There are general agreements between the emission ratios and the simulated correlation slopes for the CH_4 / CO_2 ratio, but the CO / CO_2 and CO / CH_4 emission ratios are about 20 % and 25 % lower than the simulated $\Delta CO / \Delta CO_2$ and $\Delta CO / \Delta CH_4$ correlation slopes, respectively. These higher simulated correlation slopes, despite the CO removal reaction with the OH radical in the model, can be explained by the more localized and heterogeneous distribution of CO emissions within EFA than CH_4 and CO_2.

In order to examine the influence of different emission maps on the simulated $\Delta CH_4 / \Delta CO_2$ and $\Delta CO / \Delta CO_2$ slopes, we repeat the above calculation by replacing one emission map with the ODIAC or REAS emission map (see Sect. 4.2). The results are depicted in Fig. S7. Note that since the emission maps are scaled to match the national emissions from the East Asian countries, the differences in the correlation slopes should be attributed to the differences in the emission distributions. The ODIAC CO_2 emission maps systematically produce about 4 % and 5 % lower $\Delta CH_4 / \Delta CO_2$ and $\Delta CO / \Delta CO_2$ slopes, respectively, than the EDGAR CO_2 emission maps. The $\Delta CH_4 / \Delta CO_2$ slopes based on the REAS and EDGAR emission maps agree with each other to within ± 1 %, while the $\Delta CO / \Delta CO_2$ slopes based on the REAS emission maps are systematically higher by about 2 % than those based on the EDGAR emission maps. Additionally, we simulate $\Delta CH_4 / \Delta CO_2$ and $\Delta CO / \Delta CO_2$ slopes with the 1998 EDGAR CO_2 emission map, although the national emissions had increased according to the CDIAC inventories. This caused the simulated slopes to gradually depart from those for the normal case, but the differences are less than +1 % even in 2010. The REAS CH_4 emission map systematically produces about 4 % higher $\Delta CH_4 / \Delta CO_2$ on average, while the REAS CO emission map produces about 13 % lower $\Delta CO / \Delta CO_2$ slopes. From these limited results, we take these differences in the correlation slopes as the uncertainties caused by the uncertain emission distributions: 5 % for CO_2, 4% for CH_4, and 13 % for CO.

5.3 Estimation of CH_4 and CO emissions from EFA

We estimate the year-to-year change in the emissions of CH_4 and CO from EFA so that the simulated $\Delta CH_4 / \Delta CO_2$ and $\Delta CO / \Delta CO_2$ correlation slopes match the observations. We do this by adjusting single multiplying factors for the CH_4 and CO emissions. In this estimation, we assume that the flux maps of fossil CO_2 based on the EDGAR v4.2 emission map and the CDIAC database are correct. Additionally, we also

assume, for ease of interpretation, no interannual variations in the terrestrial biospheric and oceanic CO_2 fluxes. Since the simulated correlation slopes from the annual CO_2 emissions are based on a 5 yr (2006–2010) concentration footprint calculated by FLEXPART, the annual emission estimates do not reflect the meteorological field of the corresponding years. The influence of the year-to-year variation in the meteorological condition on the simulated correlation slope is therefore part of the variability of the 5 yr simulation.

The optimized winter CH_4 and CO emissions are simply extended to annual emissions. We can do this because the CH_4 emissions from biotic sources like rice fields have large seasonality, with highest emissions occurring in the summer. In China, CH_4 emissions from rice fields occur from April to October, and more than 70 % of the total emission happens between June and August, with about 90 % of it occurring in southern China (between 23° N and 33° N) (Yan et al., 2003). Therefore, a large contribution to the observed CH_4 SSV at HAT during the winter comes from the nonseasonal CH_4 emissions from the anthropogenic sources, and not from biotic sources like the rice fields.

Interannual variations in the annual CH_4 and CO emissions are estimated using two scenarios: (1) S1 – changing the emissions from EFA; and (2) S2 – changing only the emissions from China within EFA. The estimated emissions are depicted in Fig. 8, where the results from S1 and S2 are denoted by the closed squares and open circles, respectively. The error bars in the figure represent estimated uncertainties, which consist of uncertainties associated with the observed and simulated average correlation slopes, the uncertainties associated with the correlation coefficient criteria (2.5 % for $\Delta CH_4 / \Delta CO_2$ and 2.3 % for $\Delta CO / \Delta CO_2$; see Sect. 3), the uncertainty of the fossil-fuel-derived CO_2 emissions from China (15 %; Gregg et al., 2008), and the uncertainty derived from the uncertain emission distributions (5 % for CO_2, 4 % for CH_4, and 13 % for CO; see Sect. 5.2). In Fig. 8, we also plot the Chinese part of the EFA emissions in S1 as open squares. The CH_4 emissions from China estimated in S1 and S2, shown as open circles and open squares in Fig. 8a, agree to within ±3 % of each other. Similar results can be seen in the CO emissions from China (Fig. 8b) although the Chinese CO emissions in S2 are, on average, systematically higher by about 4 % than those in S1. These results seem to suggest that the emissions from EFA outside China contribute little to the observed changes in the average correlation slopes at HAT and the emissions from the Chinese part of EFA can be robustly estimated by both scenarios.

The estimated annual CH_4 emissions are relatively stable during the first several years but increase thereafter; for CO, they seem to increase and decrease during the early part and the later part of the observation period, respectively. The annual CH_4 emission from China within EFA is about 21 $TgCH_4\,yr^{-1}$ during 1998–2005 and increases to about 27 $TgCH_4\,yr^{-1}$ in 2009/2010; but for CO it is about 100 $TgCO\,yr^{-1}$ in 1998/1999, increases to about 140 $TgCO\,yr^{-1}$ in 2004/2005, and then slightly decreases to about 120 $TgCO\,yr^{-1}$ in 2009/2010. The simulated $\Delta CO / \Delta CH_4$ slopes based on these optimized CH_4 and CO emissions from China within EFA (S2), plotted in Fig. 7c as black open squares, show considerable agreement with the observations.

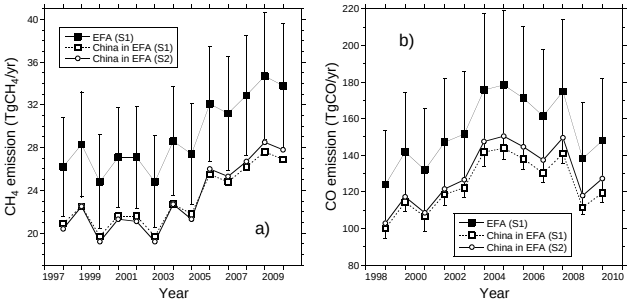

Fig. 8. Temporal changes in the estimated **(a)** CH_4 and **(b)** CO emissions from EFA. The emissions from EFA for S1 are depicted by closed squares with uncertainties. The emissions from China in EFA are depicted for S1 by open squares and for S2 by open circles (see text).

5.4 Comparison of the estimated emissions with other studies

The estimated CH_4 and CO emissions from China in the previous section are compared with the annual emissions from China estimated by other studies. Since we have optimized those Chinese emissions from EFA only (S2), we have added the emissions from China outside EFA (hereinafter referred to as the extended Chinese area (ECA)) to obtain an estimated national emission for the winter period. These additional emissions from ECA are computed from the CH_4 and CO flux maps prepared in Sect. 4.2. We thus obtain additional emissions of 18 $TgCH_4\,yr^{-1}$ and 31.6 $TgCO\,yr^{-1}$, which we assume to be constant over the study period. Our estimated CH_4 and CO emissions from China are summarized in Table 1 and plotted in Figs. 9 and 10, respectively. We find that the estimated CH_4 and CO emissions from ECA contribute less than 47 % and 23 % to the total China emissions, respectively.

5.4.1 CH_4

Bottom-up estimates of the CH_4 emission from Chinese anthropogenic sources without the rice fields taken from the inventory databases EDGAR v4.2, REAS v1.1 (Ohara et al., 2007; http://www.jamstec.go.jp/frsgc/research/p3/emission.htm) and REAS v2.1 are plotted for comparison with our results in Fig. 9. The EDGAR v4.2 emission estimates show good agreement with our estimates for the period 1998 to 2002. However, after 2002 the EDGAR v4.2 data show a much faster increase of 3.1 ± 0.1 $TgCH_4\,yr^{-2}$

Table 1. Summary of the estimated CH_4 and CO emissions from China[a].

Year	Fossil fuel CO_2[b]	CH_4[c,d]	CO[d]
1997/1998	0.93	38.4 ± 6.8	
1998/1999	0.91	40.5 ± 7.0	134 ± 32
1999/2000	0.92	37.3 ± 6.6	149 ± 34
2000/2001	0.94	39.4 ± 6.8	140 ± 35
2001/2002	0.98	39.1 ± 6.9	153 ± 36
2002/2003	1.12	37.3 ± 6.4	158 ± 36
2003/2004	1.34	40.7 ± 7.2	179 ± 42
2004/2005	1.51	39.4 ± 6.7	182 ± 42
2005/2006	1.66	44.0 ± 7.4	176 ± 40
2006/2007	1.80	43.3 ± 7.3	169 ± 38
2007/2008	1.88	44.7 ± 7.6	181 ± 41
2008/2009	1.98	46.5 ± 7.9	150 ± 33
2009/2010	2.14	45.8 ± 7.9	159 ± 36

[a]Values for CO_2 are given in PgC yr^{-1}, for CH_4 in $TgCH_4$ yr^{-1}, and for CO in TgCO yr^{-1}. [b]Fossil CO_2 emissions are taken from the CDIAC database. Each value is the average of the emissions for the consecutive two years described in the first column. The uncertainty is assumed to be 15 %, which is the lower limit of the estimation of Gregg et al. (2008). [c]Values represent the emissions from nonseasonal CH_4 sources (see text). [d]Uncertainties are calculated from the uncertainties of the fossil-fuel-derived CO_2 emissions in China, of the observed correlation slopes including the influence of the correlation coefficient criteria selection, and of the simulated correlation slopes including the influence of the uncertain emission distributions used in the simulation (see text).

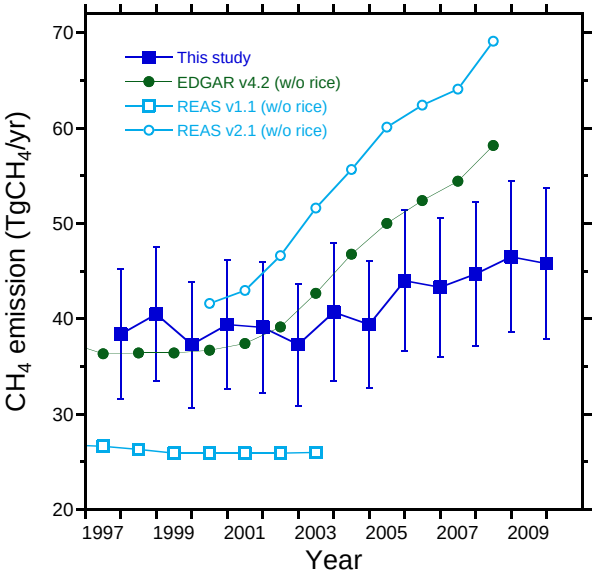

Fig. 9. Comparison of estimated nonseasonal CH_4 emissions from China. The values are expressed as annual emissions. Closed blue squares are the estimated emissions of this study. Green circles, light-blue squares, and light-blue circles represent the CH_4 emissions from anthropogenic sources (excluding rice fields) in China based on the emission inventories from EDGAR v4.2 (http://edgar.jrc.ec.europa.eu/), REAS v1.1 (Ohara et al., 2007) and REAS v2.1 (Kurokawa et al., 2013), respectively.

(2002–2008), which is about 3 times larger than our estimates of 1.1 ± 0.2 $TgCH_4$ yr^{-2} (2002–2010). The REAS v2.1 estimates, being higher than our estimates, also show a faster increase of 3.6 ± 0.2 $TgCH_4$ yr^{-2} (2000–2008). About 70 % and 90 % of the increases in the Chinese emissions in the EDGAR v4.2 and REAS v2.1 estimates, respectively, are attributed to the emissions related to coal mining (fugitive emissions from solid fuels), and occur mostly within EFA. Note that the REAS v1.1 estimates are lower than our estimates and the differences from the REAS v2.1 estimate for 2000 are attributed to the fugitive emissions from fossil fuels (73 %) and the emissions from land disposal of solid waste (24 %).

The possibility that the CH_4 emissions in the EDGAR v4.2 inventory are overestimated was also suggested by the following model studies. In a chemistry-transport model intercomparison experiment of CH_4 (TransCom-CH_4), the forward simulations of atmospheric CH_4 were conducted using several transport models and various sets of surface CH_4 emission scenarios (Patra et al., 2011). The forward CH_4 simulation based on the EDGAR v4.0 emissions, which are almost same as the EDGAR v4.2 emissions, shows a significantly faster growth rate during 2003–2007 than the observations. The Chinese emission increase contributes nearly 40 % to the global CH_4 emission increase in the EDGAR inventory. Recently, Bergamaschi et al. (2013) estimated global CH_4 emissions during the 2000s based on an inverse modeling constrained by atmospheric CH_4 data from the global air sampling network and satellite sensor. The inversion result shows a significant increase in the anthropogenic CH_4 emissions from China but a smaller increase than that indicated by the EDGAR inventory. The increasing rate of 1.1 ± 0.3 $TgCH_4$ yr^{-2} estimated by Bergamaschi et al. (2013) for the period of 2000–2010 is in excellent agreement with our estimation. Therefore, we suspect that the EDGAR v4.2 and REAS v2.1 inventories are overestimating the recent increase in the CH_4 emissions related to the coal mining.

5.4.2 CO

The reported estimates of CO emission from China based on bottom-up and top-down approaches are plotted in Fig. 10, together with our estimates. The bottom-up estimates from REAS v1.1 and EDGAR v4.2 and other studies (Streets et al., 2003, 2006; Zhang et al., 2009) are plotted as circles in the figure. The top-down approach is divided into inverse modeling (Palmer et al., 2003; Wang et al., 2004; Heald et al., 2004; Yumimoto and Uno, 2006, 2012; Tanimoto et al., 2008; Kopacz et al., 2009) and forward modeling (Heald et al., 2003; Allen et al., 2004), which are plotted as squares and diamonds in the figure, respectively. These top-down emissions were estimated by using CO observations from aircrafts, ground-based stations, satellites, or any combination

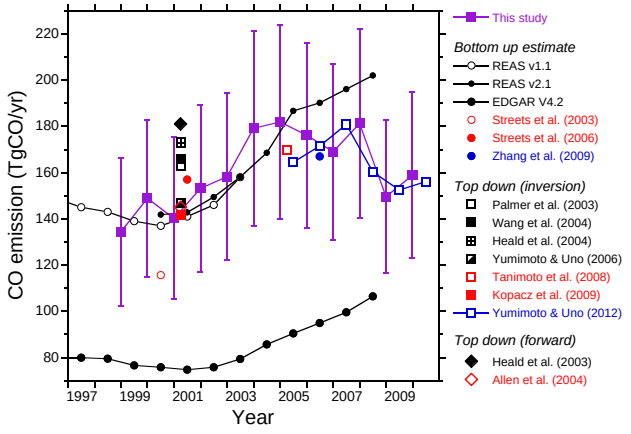

Fig. 10. Comparison of estimated CO emissions from China. The values are expressed as annual emissions. Closed blue squares are the estimated emissions of this study. Circles, squares, and diamonds represent the bottom-up estimates, top-down (inversion), and top-down (forward) estimates, respectively.

thereof. In general, our estimated emissions agree with these reported bottom-up and top-down estimations except those taken from the EDGAR v4.2 database, which shows about 40 % lower estimates than the other estimates, including ours.

The top-down estimates, including ours, reflect not only the primary CO emissions but also the secondary CO production from the oxidation of NMVOC. However, we consider the contribution of the CH_4 oxidation to the top-down estimates of CO emissions based on the atmospheric observations in the downwind regions from China to be negligible because of the much longer life time of atmospheric CH_4 (about 10 yr; e.g., Patra et al., 2011) compared to its transit time. It is to be noted that the EDGAR database reports only the primary CO emissions. Duncan et al. (2007) estimated that the oxidation of NMVOC contributes nearly 50 % of the total primary CO emissions to the global CO emission. If this ratio is valid and can be applied to the EDGAR estimate for China, then the resulting net CO emissions with both primary and secondary sources can be applied to our top-down estimates. In addition, our winter emission estimates would of course be biased if the CO emission has a noticeable seasonality. For example, using monthly data for power generation and industry, as well as residential energy consumption, Zhang et al. (2009) developed a data set of monthly CO emissions from China. The result shows a significant seasonality, with 17 % larger average monthly emission for our 5-month winter than for an entire year. If in fact there is a strong seasonal variation in the CO emission, then our winter estimate needs to be reduced by 17 %, which also brings our estimate close to the EDGAR v4.2 estimate. The above discussion points to the importance of correct evaluation of the secondary CO emissions when comparing top-down and bottom-up emission estimates. Note that the REAS v2.1 estimates, in which the secondary CO emissions are not explicitly included, agree well with the top-down estimate. Kurokawa et al. (2013) attribute the differences in the CO emissions between REAS v2.1 and EDGAR v4.2 to the emission factors used in the estimations; the emission factors for REAS v2.1 might implicitly include the secondary productions.

The TRACE-P (Transport and Chemical Evolution over the Pacific) campaign, which was intensively conducted over the western Pacific in the spring of 2001, reported several CO emission estimates from China; these values are shown in Fig. 10. Those estimates range from 142 to 181 $TgCO\,yr^{-1}$, with lower values corresponding closely to the bottom-up estimates of REAS v1.1 and v2.1 and our estimates. The year-to-year variation in our emission estimates agree with the reported variation in the emission estimates during the period 1999–2010. The CO emission increase during 1999–2005 is easily understandable because fossil fuel consumption in China has steadily increased after 2000. The question is whether the CO emission from China has truly stopped increasing after 2005 in spite of the continued increase in the estimated fossil fuel consumption.

From the atmospheric CO_2, CO and $^{14}CO_2$ measurements at Tae-Ahn Peninsula in Korea (TAP) during 2004–2010, Turnbull et al. (2011) found that the emission ratio of CO to fossil-fuel-derived CO_2 from China showed a gradual decrease during 2004–2006 and then plateaued from 2007 till 2009. For the usual 3-month winter season (December–February), Wang et al. (2010) showed that an average of the CO/CO_2 slopes observed at the Miyun site (located about 100 km northeast of Beijing), also showed a decreasing trend from the 2004/2005 winter to the 2008/2009 winter, with the latter value being slightly larger than that for the 2007/2008 winter (Wang et al., 2010). They attributed these decreasing trends in the CO/CO_2 ratio to recent improvements in the fossil fuel combustion efficiency in China, corresponding in time to the implementation of air pollution reduction measures to improve the air quality in Beijing prior to the 2008 Summer Olympics and Paralympics Games.

Although the CO/CO_2 ratio values obtained by Wang et al. (2010) and Turnbull et al. (2011) showed a slight increase after 2008, the $\Delta CO/\Delta CO_2$ slopes at HAT in 2009–2010 show a substantial decrease compared to those of the preceding years. Top-down estimates based on the satellite data from Yumimoto and Uno (2012), although showing a slight increase during 2005–2007, also show a distinct decrease from 2007 to 2008 (shown as open blue squares with line in Fig. 10) and maintain the lower values during 2008–2010. This continued decrease seems to suggest that the overall combustion efficiency in China might still continue to improve even after the Olympics. However, as we noted above, the observed temporal changes in the CO/CO_2 slopes at HAT are mainly reflective of the year-to-year variation in the terrestrial CO_2 emission strength and atmospheric transport. For example, relative increases in the air mass transport from

Korea and Japan, which have lower CO / CO_2 emission ratios than China, could reduce the $\Delta CO / \Delta CO_2$ slopes at HAT. Such issues will be examined in our future work.

6 Conclusion

We have examined the year-to-year changes in the average correlation slopes of $\Delta CH_4 / \Delta CO_2$, $\Delta CO / \Delta CO_2$ and $\Delta CO / \Delta CH_4$ for a 5-month winter from November to March observed at HAT over the last 10 yr. Consistent with the recent rapid increase in the fossil fuel CO_2 emissions from China, the observed $\Delta CH_4 / \Delta CO_2$ and $\Delta CO / \Delta CO_2$ slopes have correspondingly decreased. However, there are differences in the decreasing trends between $\Delta CH_4 / \Delta CO_2$ and $\Delta CO / \Delta CO_2$ slopes; the rate of decrease for the $\Delta CH_4 / \Delta CO_2$ slope is decreasing while that for the $\Delta CO / \Delta CO_2$ slope is increasing during the study period. These observational results may reflect differences in the interannual variations that are occurring between the emissions of CH_4 and CO from their source regions. Such different emission trends are also supported by the temporal changes observed in the $\Delta CO / \Delta CH_4$ slope, with an increasing trend during 1999–2004 and a decreasing trend during 2005–2010.

We have estimated the geographical distribution of the sensitivity of the winter measurements at HAT to the emissions from East Asia by using a Lagrangian particle dispersion model (FLEXPART) driven by meteorological data from 2006 to 2010. The average sensitivity distribution (average footprint) shows that the emissions from northern and eastern China mostly contribute to the observed short-term variations at HAT. We have also evaluated the relationship between the emissions from East Asia and the correlation slopes at HAT by using FLEXPART and a set of previously reported emission maps. From the relationship, we have been able to obtain estimates of the CH_4 and CO emissions from China so that the simulated average $\Delta CH_4 / \Delta CO_2$ and $\Delta CO / \Delta CO_2$ slopes would match the observed slopes. In this calculation, we have assumed that there are no year-to-year variations in the land biotic and oceanic CO_2 emissions and that the fossil-fuel-derived CO_2 emissions change in accordance with the CDIAC database. The estimated CH_4 emissions from China, corresponding to emissions from nonseasonal sources or anthropogenic sources without rice fields, show a relatively constant value of about $39 \pm 7\,TgCH_4\,yr^{-1}$ during 1998–2002, gradually increasing at a rate of $1.1 \pm 0.2\,TgCH_4\,yr^{-2}$ during 2002–2010, and then reaching $46 \pm 8\,TgCH_4\,yr^{-1}$ in 2009/2010. This increasing rate of the Chinese CH_4 emissions for the decadal period under study is much smaller than those taken from the EDGAR v4.2 and REAS v2.1 databases. However, these estimated CH_4 emission increases are not negligible in the context of the global CH_4 budget, and might substantially contribute to the recent atmospheric CH_4 increase (Rigby et al., 2008; Dlugokencky et al., 2009; Terao et al., 2011).

We have estimated the annual CO emissions from China to be $134 \pm 32\,TgCO\,yr^{-1}$ in 1998/1999, increasing to $182 \pm 42\,TgCO\,yr^{-1}$ in 2004/2005, plateauing during 2005–2008, and then decreasing to less than $160\,TgCO\,yr^{-1}$ after 2008/2009. In spite of the recent continued increase in fossil fuel consumption in China, our results have shown that the recent stagnation or decrease in the CO emission from China points to the possibility of a continued improvement in the combustion efficiency in that country due to air pollution reduction measures that were implemented prior to the 2008 Olympics. Our CO emission estimates agree well with previously reported CO emission estimates, except for the EDGAR v4.2 database, which shows a value smaller than our estimates by about $30\,TgCO\,yr^{-1}$. However, this discrepancy may be attributed to the secondary CO production derived from the atmospheric oxidation of NMVOC, which is not included in the EDGAR bottom-up estimation.

Supplementary material related to this article is available online at http://www.atmos-chem-phys.net/14/1663/2014/acp-14-1663-2014-supplement.pdf.

Acknowledgements. We gratefully acknowledge N. Oda and other members of the Global Environment Forum and the staff of the Center for Global Environmental Research for their continued support in maintaining the in situ measurements of CO_2, CH_4 and CO at HAT. We also thank H. Sandanbata and Y. Kajita for the preparation and measurement of flask samples collected at HAT. Thanks are also expressed to I. Uno and K. Yumimoto for helpful discussions on the temporal change in the CO emissions from China and to T. Oda for helpful discussions on the global fossil fuel CO_2 emission data sets. Two anonymous reviewers made valuable comments, which helped to improve the manuscript considerably.

Edited by: C. Gerbig

References

Allen, D., Pickering, K., and Fox-Rabinovitz, K.: Evaluation of pollutant outflow and CO sources during TRACE-P using model-calculated, aircraft-based, and Measurements of Pollution in the Troposphere (MOPITT)-derived CO concentrations, J. Geophys. Res., 109, D15S03, doi:10.1029/2003JD004250, 2004.

Bergamaschi, P., Houweling, S., Segers, A., Krol, M., Frankenberg, C., Scheepmaker, R. A., Dlugokencky, E., Wofsy, S. C., Kort, E. A., Sweeney, C., Schuck, T., Brenninkmeijer, C., Chen, H., Beck, V., and Gerbig, C.: Atmospheric CH_4 in the first decade of the 21st century: inverse modeling analysis using SCIAMACHY satellite retrievals and NOAA surface measurements, J. Geophys. Res.-Atmos., 118, 7350–7369, doi:10.1002/jgrd.50480, 2013.

Boden, T. A., Marland, G., and Andres, R. J.: Global, regional, and national fossil-fuel CO_2 emissions, Carbon Dioxide Information Analysis Center, Oak Ridge National Labo-

ratory, US Department of Energy, Oak Ridge, Tenn., USA, doi:10.3334/CDIAC/00001, 2011.

Dlugokencky, E. J., Masarie, K. A., Lang, P. M., and Tans, P. P.: Continuing decline in the growth rate of the atmospheric methane burden, Nature, 393, 447–450, 1998.

Dlugokencky, E. J., Houweling, S., Bruhwiler, L., Masarie, K. A., Lang, P. M., Miller, J. B., and Tans, P. P.: Atmospheric methane levels off: Temporary pause or a new steady-state?, Geophys. Res. Lett., 30, 1992, doi:10.1029/2003GL018126, 2003.

Dlugokencky, E. J., Bruhwiler, L, White, J. W. C., Emmons, L. K., Novelli, P. C., Montzka, S. A., Masarie, K. A., Lang, P. M., Crotwell, A. M., Miller, J. B., and Gatti, L. V.: Observational constraints on recent increases in the atmospheric CH_4 burden, Geophys. Res. Lett., 36, L18803, doi:10.1029/2009GL039780, 2009.

Duncan, B. N., Logan, J. A., Bey, I., Megretskaia, I. A., Yantosca, R. M., Novelli, P. C., Jones, N. B., and Rinsland, C. P.: Global budget of CO, 1988–1997: Source estimates and validation with a global model, J. Geophys. Res., 112, D22301, doi:10.1029/2007JD008459, 2007.

EC-JRC/PBL: European Commission, Joint Research Center/Netherlands Environmental Assessment Agency, Emission Database for Global Atmospheric Research (EDGAR), release version 4.2, available at: http://edgar.jrc.ec.europa.eu/index.php (last access: 4 October 2012), 2011.

Etheridge, D. M., Steele, L. P., Francy, R. J., and Langenfelds, L.: Atmospheric methane between 100 A. D. and present: Evidence of anthropogenic emissions and climatic variability, J. Geophys. Res., 103, 15979–15993, 1998.

Ganshin, A., Oda, T., Saito, M., Maksyutov, S., Valsala, V., Andres, R. J., Fisher, R. E., Lowry, D., Lukyanov, A., Matsueda, H., Nisbet, E. G., Rigby, M., Sawa, Y., Toumi, R., Tsuboi, K., Varlagin, A., and Zhuravlev, R.: A global coupled Eulerian-Lagrangian model and 1×1 km CO_2 surface flux dataset for high-resolution atmospheric CO_2 transport simulations, Geosci. Model Dev., 5, 231–243, doi:10.5194/gmd-5-231-2012, 2012.

Ganshin, A. V., Zhuravlev, R. V., Maksyutov, S., Lukyanov, A. N., and Mukai, H.: Simulation of contribution of continental anthropogenic sources to variations in the CO_2 concentration during winter period on Hateruma Island, Atmos. Ocean. Opt., 26, 35–40, 2013.

Gregg, J. S., Andres, R. J., and Marland, G.: China: Emissions pattern of the world leader in CO_2 emissions from fossil fuel consumption and cement production, Geophys. Res. Lett., 35, L08806, doi:10.1029/2007GL032887, 2008.

Heald, C. L., Jacob, D. J., Fiore, A. M., Emmons, L. K., Gille, J. C., Deeter, M. N., Warner, J., Edwards, D. P., Crawford, J. H., Hamlin, A. J., Sachse, G. W., Browell, E. V., Avery, M. A., Vay, S. A., Westberg, D. J., Blake, D. R., Singh, H. B., Sandholm, S. T., Talbot, R. W., and Fuelberg, H. E.: Asian outflow and tran-integrated satellite, aircraft, and model perspective, J. Geophys. Res., 108, 4804, doi:10.1029/2003JD003507, 2003.

Heald, C. L., Jacob, D. J., Jones, D. B. A., Palmer, P. I., Logan, J. A., Streets, D. G., Sachse, G. W., Gille, J. C., Hoffman, R. N., and Nehrkorn, T.: Comparative inverse analysis of satellite (MOPITT) and aircraft (TRACE-P) observations to estimate Asian sources of carbon monoxide, J. Geophys. Res., 109, D23306, doi:10.1029/2004JD005185, 2004.

Hirsch, R. M. and Gilroy, E. J.: Methods of fitting a straight line to data: Examples in water resources, Water Resour. Bull., 20, 705–711, 1984.

Katsumata, K., Machida, T., Tanimoto, H., Nara, H., and Mukai, H.: Re-evaluation of NIES CO scale using high concentration gravimetric CO standard gases, Paper presented at: Report of the 15th WMO Meeting of Experts on Carbon Dioxide Concentration and Related Tracer Measurement Techniques; September 2009; Jena, Germany, (WMO/GAW Rep. 194, edited by: Brand, W., 295–298, WMO, Geneva, Switzerland), 2011.

Kopacz, M., Jacob, D. J., Henze, D. K., Heald, C. L., Streets, D. G., and Zhang, Q.: Comparison of adjoint and analytical Bayesian inversion methods for constraining Asian sources of carbon monoxide using satellite (MOPITT) measurements of CO columns, J. Geophys. Res., 114, D04305, doi:10.1029/2007JD009264, 2009.

Koyama, Y., Maksyutov, S., Mukai, H., Thoning, K., and Tans, P.: Simulation of variability in atmospheric carbon dioxide using a global coupled Eulerian – Lagrangian transport model, Geosci. Model Dev., 4, 317–324, doi:10.5194/gmd-4-317-2011, 2011.

Kurokawa, J., Ohara, T., Morikawa, T., Hanayama, S., Janssens-Maenhout, G., Fukui, T., Kawashima, K., and Akimoto, H.: Emissions of air pollutants and greenhouse gases over Asian regions during 2000–2008: Regional Emission inventory in ASia (REAS) version 2, Atmos. Chem. Phys., 13, 11019–11058, doi:10.5194/acp-13-11019-2013, 2013.

Levin, I., Kromer, B., Schmidt, M.,, and Sartorius, H.: A novel approach for independent budgeting of fossil fuel CO_2 over Europe by $^{14}CO_2$ observations, Geophys. Res. Lett., 30, 2194, doi:10.1029/2003GL018477, 2003.

Logan, J. A., Prather, M. J., Wofsy, S. C., and McElroy, M. B.: Tropospheric chemistry-A global perspective, J. Geophys. Res., 104, 26245–26277, 1981.

Machida, T., Tohjima, Y., Katsumata, K., and Mukai, H.: A new CO_2 calibration scale based on gravimetric one-step dilution cylinders in National Institute for Environmental Studies-NIES09 CO_2 scale. Paper presented at: Report of the 15th WMO Meeting of Experts on Carbon Dioxide Concentration and Related Tracer Measurement Techniques; September2009; Jena, Germany, (WMO/GAW Rep. 194, edited by: Brand, W., 165–169, WMO, Geneva, Switzerland), 2011.

Maksyutov, S., Takagi, H., Valsala, V. K., Saito, M., Oda, T., Saeki, T., Belikov, D. A., Saito, R., Ito, A., Yoshida, Y., Morino, I., Uchino, O., Andres, R. J., and Yokota, T.: Regional CO_2 flux estimates for 2009–2010 based on GOSAT and ground-based CO_2 observations, Atmos. Chem. Phys., 13, 9351–9373, doi:10.5194/acp-13-9351-2013, 2013.

Minejima, C., Kubo, M., Tohjima, Y., Yamagishi, H., Koyama, Y., Maksyutov, S., Kita, K., and Mukai, H.: Analysis of $\Delta O_2/\Delta CO_2$ ratios for the pollution events observed at Hateruma Island, Japan, Atmos. Chem. Phys., 12, 2713–2723, doi:10.5194/acp-12-2713-2012, 2012.

Mukai, H., Katsumoto, M., Ide, R., Machida, T., Fujinuma, Y., Nojiri, Y., Inagaki, M., Oda, N., and Watai. T.: Characterization of atmospheric CO_2 observed at two-background air monitoring stations (Hateruma and Ochi-ishi) in Japan. Paper presented at: Sixth International Carbon Dioxide Conference; October 2001; Sendai, Japan, 2001.

Nakatsuka, Y. and Maksyutov, S.: Optimization of the seasonal cycles of simulated CO_2 flux by fitting simulated atmospheric CO_2 to observed vertical profiles, Biogeosciences, 6, 2733–2741, doi:10.5194/bg-6-2733-2009, 2009.

Nakazawa, T., Machida, T., Tanaka, M., Fujii, Y., Aoki, S., and Watanabe, O.: Differences of the atmospheric CH_4 concentration between the Arctic and Antarctic regions in pre-industrial/pre-agricultural era, Geophys. Res. Lett., 20, 943–946, 1993.

Oda, T. and Maksyutov, S.: A very high-resolution (1 km × 1 km) global fossil fuel CO_2 emission inventory derived using a point source database and satellite observations of nighttime lights, Atmos. Chem. Phys., 11, 543–556, doi:10.5194/acp-11-543-2011, 2011.

Ohara, T., Akimoto, H., Kurokawa, J., Horii, N., Yamaji, K., Yan, X., and Hayasaka, T.: An Asian emission inventory of anthropogenic emission sources for the period 1980–2020, Atmos. Chem. Phys., 7, 4419–4444, doi:10.5194/acp-7-4419-2007, 2007.

Palmer, P. I., Jacob, D. J., Jones, D. B. A., Heald, C. L., Yantosca, R. M., Logan, J. A., Sachse, G. W., and Streets, D. G.: Inverting for emissions of carbon monoxide from Asia using aircraft observations over the western Pacific, J. Geophys. Res., 108, 8828, doi:10.1029/2003JD003397, 2003.

Patra, P. K., Takigawa, M., Ishijima, K., Choi, B.-C., Cunnold, D., Dlugokencky, E. J., Fraser, P., Gomez-Pelaez, A. J., Goo, T.-Y., Kim, J.-S., Krummel, P., Langenfelds, R., Meinhardt, F., Mukai, H., O'Doherty, S., Prinn, R. G., Simmonds, P., Steele, P., Tohjima. Y., Tsuboi, K., Uhse, K., Weiss, R., Worthy, D., and Nakazawa, T.: Growth rate, seasonal, synoptic, diurnal variations and budget in lower atmospheric methane, J. Meteorol. Soc. Jpn., 87, 635–663, doi:10.2151/jmsj.87.635, 2009.

Patra, P. K., Houweling, S., Krol, M., Bousquet, P., Belikov, D., Bergmann, D., Bian, H., Cameron-Smith, P., Chipperfield, M. P., Corbin, K., Fortems-Cheiney, A., Fraser, A., Gloor, E., Hess, P., Ito, A., Kawa, S. R., Law, R. M., Loh, Z., Maksyutov, S., Meng, L., Palmer, P. I., Prinn, R. G., Rigby, M., Saito, R., and Wilson, C.: TransCom model simulations of CH_4 and related species: linking transport, surface flux and chemical loss with CH_4 variability in the troposphere and lower stratosphere, Atmos. Chem. Phys., 11, 12813–12837, doi:10.5194/acp-11-12813-2011, 2011.

Rigby, M., Prinn, R. G., Fraser, P. J., Simmonds, P. G., Langenfelds, R. L., Huang, J., Cunnold, D. M., Steele, L. P., Krummel, P. B., Weiss, R. F., O'Doherty, S., Salameh, P. K., Wang, H. J., Harth, C. M., Mühle, J., and Porter, L., W.: Renewed growth of atmospheric methane. Geophys. Res. Lett. 35, L22805, doi:10.1029/2008GL036037, 2008.

Sander, S. P., Friedl, R. R., Golden, D. M., Kuryolo, M. J., Moortgat, G. K., Keller-Rudek, H., Wine, P. H., Ravishankara, A. R., Kolb, C. E., Molina, M. J., Finlayson-Pitts, B. J., Huie, R. E., and Orkin, V. L.: Chemical kinetics and photochemical data for use in atmospheric studies, Jet Propul. Lab., Pasadena, CA, Rep. 06-2, 523 pp., 2006.

Schmidt, M., Graul, R., Sartorius, H., and Levin, I.: The Schauinsland CO_2 record: 30 years of continental observations and their implications for the variability of the European CO_2 budget, J. Geophys. Res., 108, 4619, doi:10.1029/2002JD003085, 2003.

Spivakovsky, C. M., Logan, J. A., Montzka, S. A., Balkanski, Y. J., Foreman-Fowler, M., Jones, B. A., Horowitz, L. W., Fusco, A. C., Brenninkmeijer, C. A. M., Prather, M. J., Wofsy, S. C., and McElroy, M. B.: Three dimensional climatological distribution of tropospheric OH: Update and evaluation, J. Geophys. Res., 105, 8931–8980, doi:10.1029/1999JD901006, 2000.

Steele, L. P., Dlugokencky, E. J., Lang, P. M., Tans, P. P., Martin, R. C., and Masarie, K. A.: Slowing down of the global accumulation of atmospheric methane during the 1980's, Nature, 358, 313–316, 1992.

Stohl, A., Hittenberger, M., and Wotawa, G.: Validation of the Lagrangian particle dispersion model FLEXPART against large-scale tracer experiment data, Atmos. Environ., 32, 4245–4264, 1998.

Streets, D. G., Bond, T. C., Carmichael, G. R., Fernandes, S. D., Fu, Q., He, D., Klimont, Z., Nelson, S. M., Tsai, N. Y., Wang, M. Q., Woo, J.-H., and Yarber, K. F.: An inventory of gaseous and primary aerosol emissions in Asia in the year 2000, J. Geophys. Res., 108, 8809, doi:10.1029/2002JD003093, 2003.

Streets, D. G., Zhang, Q., Wang, L., He, K., Hao, J., Wu, Y., Tang, Y., and Carmichael, G. R.: Revisiting China's CO emissions after the Transport and Chemical Evolution over the Pacific (TRACE-P) mission: Synthesis of inventories, atmospheric modeling, and observations, J. Geophys. Res., 111, D14306, doi:10.1029/2006JD007118, 2006.

Tanimoto, H., Sawa, Y., Yonemura, S., Yumimoto, K., Matsueda, H., Uno, I., Hayasaka, T., Mukai, H., Tohjima, Y., Tsuboi, K., and Zhang, L.: Diagnosing recent CO emissions and ozone evolution in East Asia using coordinated surface observations, adjoint inverse modeling, and MOPITT satellite data, Atmos. Chem. Phys., 8, 3867–3880, doi:10.5194/acp-8-3867-2008, 2008.

Takahashi, T., Sutherland, S. C., Wanninkhof, R., Sweeney, C., Feely, R. A., Chipman, D. W., Hales, B., Friederich, G., Chavez, F., Sabine, C., Watson, A., Bakker, D. C. E., Schuster, U., Metzl, N., Yoshikawa-Inoue, H., Ishii, M., Midorikawa, T., Nojiri, Y., Körtzinger, A., Steinhoff, T., Hoppema, M., Olafsson, J., Arnarson, T. S., Tilbrook, B., Johannessen, T., Olsen, A., Bellerby, R., Wong, C. S., Delille, B., Bates, N. R., and de Baar, H. J. W.: Climatological mean and decadal change in surface ocean pCO_2, and net sea-air CO_2 flux over the global oceans, Deep-Sea Res. II, 56, 554–577, doi:10.1016/j.dsr2.2008.12.009, 2009.

Tanimoto, H., Tohjima, Y., Mukai, H., Nara, H., and Hashimoto, S.: Anomalous geographical gap in carbon monoxide mixing ratios over Hokkaido (Japan) in summer 2004, Geochem. J., 43, e23–e29, 2009.

Terao, Y., Mukai, H., Nojiri, Y., Machida, T., Tohjima, Y., Saeki, T., and Maksyutov, S.: Interannual variability and trends in atmospheric methane over the western Pacific from 1994 to 2010, J. Geophys. Res., 116, D14303, doi:10.1029/2010JD015467, 2011.

Thompson, A. M.: The oxidizing capacity of the Earth's atmosphere-Probable past and future changes, Science, 256, 1157–1165, 1992.

Thoning, K., Tans, P. P., and Komhyr, W. D.: Atmospheric carbon dioxide at Mauna Loa Observatory 2. Analysis of the NOAA GMCC data, 1974–1985, J. Geophys. Res., 94, 8549–8565, 1989.

Tohjima, Y., Machida, T., Utiyama, M., Katsumoto, M., Fujinuma, Y., and Maksyutov, S.: Analysis and presentation of in situ atmospheric methane measurements from Cape Ochi-ishi and Hateruma Island, J. Geophys. Res., 107, D12, doi:10.1029/2001JD001003, 2002.

Tohjima, Y., Mukai, H., Nojiri, Y., Yamagishi, H., and Machida, T.: Atmospheric O_2/N_2 measurements at two Japanese sites: Estimation of global oceanic and land biotic carbon sinks and analysis of the vaiations in atmospheric potential oxygen (APO), Tellus, 60, 213–225, doi:10.1111/j.1600-0889.2007.00334.x, 2008.

Tohjima, Y., Mukai, H., Hashimoto, S., and Patra, P. K.: Increasing synoptic scale variability in atmospheric CO_2 at Hateruma Island associated with increasing East-Asian emissions, Atmos. Chem. Phys., 10, 453–462, doi:10.5194/acp-10-453-2010, 2010.

Turnbull, J. C., Tnas, P. P., Lehman, S. J., Baker, D., Conway, T. J., Chung, Y. S., Gregg, J., Miller, J. B., Southon, J. R, and Zhou, L.-X.: Atmospheric observations of carbon monoxide and fossil fuel CO_2 emissions from East Asia, J. Geohys. Res., 116, D24306, doi:10.1029/2011JD016691, 2011.

Wada, A, Matsueda, H., Murayama, S., Taguchi, S., Hirao, S., Yamazawa, H., Moriizumi, J., Tsuboi, K., Niwa, Y., and Sawa, Y.: Quantification of emission estimates of CO_2, CH_4 and CO for East Asia derived from atmospheric radon-222 measurements over the western North Pacific, Tellus B, 65, 18037, doi:10.3402/tellusb.v65i0.18037, 2013.

Wang, Y., Munger, J. W., Xu, S., McElroy, M. B., Hao, J., Nielsen, C. P., and Ma, H.: CO_2 and its correlation with CO at a rural site near Beijing: implications for combustion efficiency in China, Atmos. Chem. Phys., 10, 8881–8897, doi:10.5194/acp-10-8881-2010, 2010.

Wang, Y. X., McElroy, M. B., Wang, T., and Palmer, P. I.: Asian emissions of CO and NO_x: Constraints from aircraft and Chinese station data, J. Geophys. Res., 109, D24304, doi:10.1029/2004JD005250, 2004.

Worthy, D. E. J., Chan, E., Ishizawa, M., Chan, D., Poss, C., Dlugokencky, E. J., Maksyutov, S., and Levin, I.: Decreasing anthropogenic methane emissions in Europe and Siberia inferred from continuous carbon dioxide and methane observations at Alert, Canada, J. Geophys. Res., 114, D10301, doi:10.1029/2008JD011239, 2009.

Yan, X., Cai, Z., Ohara, T., and Akiomoto, H.: Methane emission from rice fields in mainland China: Amount and seasonal and spatial distribution, J. Geohys, Res., 108, 4005, doi:10.1029/2002JD003182, 2003.

Yokouchi, Y., Taguchi, S., Saito, T., Tohjima, Y., Tanimoto, H., and Mukai, H.: High frequency measurements of HFCs at a remote site in east Asia and their implications for Chinese emissions, Geophys, Res. Lett., 33, L21814, doi:10.1029/2006GL026403, 2006.

Yumimoto, K. and Uno, I.: Adjoint inverse modeling of CO emissions over the East Asian region using four dimensional variational data assimilation, Atmos. Environ., 40, 6836–6845, 2006.

Yumimoto, K. and Uno, I.: Inverse estimate of long-term CO emission in China between 2005–2010 with Green's Function Method, J. Japan. Soc. Atmos. Environ., 47, 162–172, 2012 (in Japanese with English abstract).

Zhang, Q., Streets, D. G., Carmichael, G. R., He, K. B., Huo, H., Kannari, A., Klimont, Z., Park, I. S., Reddy, S., Fu, J. S., Chen, D., Duan, L., Lei, Y., Wang, L. T., and Yao, Z. L.: Asian emissions in 2006 for the NASA INTEX-B mission, Atmos. Chem. Phys., 9, 5131–5153, doi:10.5194/acp-9-5131-2009, 2009.